A Rainfall Estimation with the GMS-5 Infrared Split-Window and Water Vapour Measurements

Toshiyuki Kurino

Meteorological Satellite Center, Japan Meteorological Agency,
3-235 Nakakiyoto, Kiyose-shi, Tokyo 204, Japan

(Received November 19, 1996 ; revised version accepted December 16, 1996)

Abstract

This paper describes statistical characteristics of an infrared (IR) rainfall estimation using the Japanese geosynchronous satellite, Geostationary Meteorological Satellite-5 (GMS-5). For this study, geographically matched data sets of the GMS-5 IR data and composite digital weather radar data were prepared. Three parameters derived from the GMS-5 IR data (IR 11 μm brightness temperature (TB_{11}) ; IR TB difference between 11 μm and 12 μm (TB_{11-12}) ; and IR TB difference between 11 μm and 6.7 μm ($TB_{11-6.7}$)) were compared with the radar observations pixel by pixel. In the case study, the following characteristics of the "GMS-5 IR—rainfall" relationship are extracted.

- TB_{11-12} is a useful parameter for removing thin cirrus with no rainfall
- $TB_{11-6.7}$ is a useful parameter for extracting deep convective cloud with heavy rainfall

By using those data sets, the GMS-5 IR data were "trained" to recognize raining pixel and its intensity based on radar observations as a ground truth, so that 3-dimensional (TB_{11}, TB_{11-12} and $TB_{11-6.7}$) matrices were constructed to relate GMS-5 IR data to probability of rain (PoR) and mean rain rate (mRR). Those matrices were used to develop an empirical technique to estimate the rain rate (RR ; RR = PoR * mRR). The potential of this technique, denoted as 3-D looking-up table (LUT), as a now casting tool for severe weather was tested in the case of typhoon "RYAN (T9514)". The error and scatter of the 3-D LUT estimations were relatively large, but they captured peak rainfalls and accumulative rainfall in good agreement.

1. Introduction

Many attempts have been made for the estimation of rainfall from geosynchronous satellite IR data, in spite of its disadvantages that rainfall is indirectly inferred from cloud observations and that the techniques are not readily transferable from the location where it is calibrated to other locations (e.g. Griffith, W.L. Woodley, P.G. Grube, D.W. Martin, J. Stout and D.N. Sikdar., 1978, Arkin and Meisner, 1987 and Adler and Negri, 1988). The reason for this is the short duration and high temporal variability of rainfall events and, therefore, only the geosynchronous satellite is able to provide IR image data with high frequency, generally less than one hour.

In Japan, the need for high temporal resolution in the rainfall observation is also strong by weather forecasters for not only forecasting but

also now casting, especially in the case of severe storm watch like a typhoon. This paper describes a new method of rainfall estimation, which identifying both of thin cirrus cloud with no rainfall and deep convective cloud with heavy rainfall, from the GMS-5 IR channels data.

2. Characteristics of the GMS-5 IR Observation

The GMS-5 has been the operational satellite at 140° E since June 21, 1995. It has produced high temporal resolution of one hour in the IR observations with spatial resolution of 5 km at the sub-satellite point. It is equipped with the Visible and Infrared Spin Scan Radiometer (VISSR), with three new IR sensors, namely a water vapour channel (6.7 ㎛) and split window channels (11 ㎛ and 12 ㎛). A noise equivalent delta temperature (NEΔT) of the split window channels is within 0.35K at 300K and 1.0K at 220K respectively. The NEΔT of the water vapour channel is within 0.22K at 300K and 1.5K at 220K.

3. Case Study

Characteristics of the GMS-5 IR data for rainfall estimation were first investigated for Okinawa Islands and surrounding oceanic regions (120-125° E, 20-35° N) with grid resolution of 0.05° for the case of typhoon "RYAN (T9514) at 00 UTC, 23 September 1995. Figure 1 shows the region of the case study. Figure 2.1, 2.2 and 2.3 show IR "false-color" images of TB_{11}, TB_{11-12} and $TB_{11-6.7}$ respectively at 00 UTC on 23 September 1995. In this case study, the GMS-5 IR data sets were compared pixel by pixel with a geographically matched composite radar data set in the same grid resolution. The radar data was obtained through Japan Meteorological Agency (JMA) weather radar network on operational basis. As a total, 29,939 pixels, including 1,373 "raining" pixels, were obtained in this case study. Figure 3 shows a false-color image of digitized echo intensity for 16 levels. It should be noted that there was time lag of 20 minutes between the satellite and radar observations.

(1) IR split window channels

In the use of IR split window channels for cloud classification, Inoue (1987a) showed the feasibility of cirrus (Ci) detection using split-window channel data from the Advanced Very High Resolution Radiometer (AVHRR) on board the NOAA polar orbiting satellites. This method is based on a threshold technique in the two-dimensional (2-D) histogram whose axes are the TB_{11} and TB_{11-12}, and Ci is identified as TB_{11-12} in the range more than 2.5°. Inoue (1987b) also showed convective rain area delineation using the split window. This finding was applied to the GMS-5 IR data in this case study. As is shown in Figure 2.1 and 2.2, the areas whose TB_{11-12} are more than or equal to 3.0° (red areas) correspond to thin fibrous Ci streaks flowing away from the typhoon. Those areas are also corresponding to no echo region in Fig. 3. Figure 4.1 is a scatter diagram of the TB_{11} and TB_{11-12} for raining pixels from radar observation. Though there are 87 (6%) raining pixels in the area whose TB_{11-12} are more than or equal to 3.0°, 1,286 (94%) pixels are belonging to the smaller TB_{11-12} differences less than 3.0°. One of the reasons for the disagreement of 87 pixels is due to the time lag of the observations between satellite and radar.

(2) IR water vapour channel

From the inspection of Figure 2.1 and 2.3, the areas whose $TB_{11-6.7}$ are less than or equal to 0.0° (blue color) correspond to deep convective clouds in the cold mass of thick upper cloud of the central region of the typhoon (a), intense

convective region of cloud clusters (b) and tapering cloud (c) in Figure 2.3. Figure 4.2 is a scatter diagram of the TB_{11} and $TB_{11-6.7}$ for "heavy (over 20.0 ㎜/hr)" rain pixels from radar observation. Though there is no definite distribution differences at $TB_{11-6.7}$ of 0.0°, 235 (90%) pixels are belonging to the smaller $TB_{11-6.7}$ differences less than 10.0°. Ackerman (1996) studied negative brightness temperature differences between 11 ㎛ and 6.7 ㎛. He theoretically showed that thick clouds produce negative differences that are typically greater than -5K for the Tropics and midlatitudes. My findings are consistent with his study. One of the reasons for the disagreement of 11 pixels whose $TB_{11-6.7}$ are more than 20.0° and TB_{11} more than 260.0K is also due to the time lag of the observations.

(3) Finding Results

From the case study, the characteristics of the GMS-5 IR channels data and radar rainfall are summarized as follows:

- TB_{11-12} is a useful parameter for removing thin cirrus with no rainfall
- $TB_{11-6.7}$ is a useful parameter for extracting deep convective cloud with heavy rainfall

4. Statistical Characteristics of the GMS-5 IR Data

Based on the above findings in the case study of the GMS-5, statistical characteristics of the GMS-5 IR channels data for estimating rainfall were extracted from a training of the GMS-5 IR TBs with radar data using the data sets described in the following section.

(1) The Data Sets

Geographically matched 6-hourly (00, 06, 12 and 18 UTC) observation data sets of the GMS -5 IR TBs (6.7 ㎛, 11 ㎛ and 12 ㎛) and a composite digital radar data set over Okinawa Islands and surrounding oceanic regions (120-135°E, 20-35°N) with 0.05° grid resolution (same as the case study) during the summer season (21 July—20 September 1995) were prepared. The radar data was obtained by JMA weather radar network on an operational basis and converted to rain rates (㎜/hr) from digitized echo intensity for 16 levels. As a total of 248 cases were prepared for this statistics. There was no compensation of the time lag between the satellite and radar observations.

(2) 3-D Matrices

For all the data sets, the GMS-5 IR data of TB_{11}, TB_{11-12} and $TB_{11-6.7}$ were compared pixel by pixel with the radar data in the same way as the case study. At first, "rain" and "no-rain" frequencies (Nr and Nnr) and total rain rate (tRR) were calculated as a function of the three variables for each pixel of the GMS-5 IR imagery using radar data. For the construction of the histograms of Nr, Nnr and tRR, denoted as 3-D histograms, TB_{11} was divided into 26 classes from 20.0°C to −105.0°C in every 2.5°C, TB_{11-12} was divided into 21 classes from −10.0°C to 9.0°C in every 1.0°C, and $TB_{11-6.7}$ was divided into 21 classes from −10.0°C to 28.0°C in every 2.0°C. Two matrices of probability of rain (PoR) and mean rain rate (mRR), denoted as 3-D matrices, were calculated from the 3-D histograms, where the input variables consisted of the same TB_{11}, TB_{11-12} and $TB_{11-6.7}$ as the 3-D histograms.

The following definitions were adopted:

$$\begin{aligned}\mathrm{PoR}(TB_{11}, TB_{11-12}, TB_{11-6.7}) &= \mathrm{Nr}(TB_{11}, TB_{11-12}, TB_{11-6.7}) \\ &\quad / (\mathrm{Nnr}(TB_{11}, TB_{11-12}, TB_{11-6.7}) \\ &\quad + \mathrm{Nr}(TB_{11}, TB_{11-12}, TB_{11-6.7}))\end{aligned}$$

$$\begin{aligned}\mathrm{mRR}(TB_{11}, TB_{11-12}, TB_{11-6.7}) &= \mathrm{tRR}(TB_{11}, TB_{11-12}, TB_{11-6.7})\end{aligned}$$

$$/Nr(TB_{11}, TB_{11-12}, TB_{11-6.7})$$

The results are shown in the form of 2-D matrices, where the input variables are consisted of (TB_{11}, TB_{11-12}) and (TB_{11}, $TB_{11-6.7}$), in tables 1 and 2.

(3) Finding Results

The resulting statistical characteristics derived from the 3-D matrices are as follows: As shown in Tables 1a and 1b, PoR generally increases with TB_{11-12} decreases and with TB_{11} decreases. Relatively high values (larger than or equal to 40%) of PoRs appear in the region of TB_{11-12} less than 3.0° and TB_{11} colder than or equal to −55.0°C. It should be noted that high PoRs (more than or equal to 55%) and high mRRs (more than 10 ㎜/h) appear in TB_{11-12} less than or equal to −1.0° even in the warmer TB_{11} up to 10.0°C. As shown in Tables 2a and 2b, PoR generally increases with $TB_{11-6.7}$ decrease. Relatively high PoR values (more than 55%) appear in the region of $TB_{11-6.7}$ less than or equal to 0.0° and TB_{11} colder than −30.0°C. There is no clear relationship for mRR in the 2-D matrix of TB_{11} and $TB_{11-6.7}$. However, the higher mRR (greater than 10.0 ㎜/hr) corresponds to the colder TB_{11} (less than −60.0°C) and the smaller $TB_{11-6.7}$ (less than 10.0°) with some exceptions.

5. The GMS-5 IR Technique for Estimating Rainfall

(1) 3-D Look-up Table

An empirical rainfall estimation algorithm (denoted as 3-D LUT) which is based on the 3-D matrices of mRR and PoR was developed. The following equation was used for estimating rainfall.

$$RR = mRR(TB_{11}, TB_{11-12}, TB_{11-6.7}) * PoR(TB_{11}, TB_{11-12}, TB_{11-6.7})$$

(2) Validation of the technique

The 3-D LUT algorithm were applied and tested on hourly scales for the case of typhoon "RYAN (T9514)" from 22 through 23 September 1995. Two 1°×1° latitude/longitude area centered at (26.5°N, 127.5°E) and (25.5°N, 128.5°E) in Figure 1 on the route of the typhoon were selected for this validation. Comparisons of rainfall estimation and radar observation as a ground truth, over the two 1°×1° area of "A" and "B" from 12 UTC on September 22 through 12 UTC on September 23 are shown in Figures 5 and 6 respectively. Hourly (a) and accumulative (b) rainfalls are shown in the figure. Rain estimations from two other techniques, CST technique described by Adler and Negri (1988), denoted as CST, and GPI technique described by Arkin and Meisner (1987), denoted as GPI, are also shown for comparison. In general, the error and scatter of all the IR hourly estimates are relatively large. It should be noted that this 3-D LUT technique is based on the 3-D matrices derived from a large statistical sample of radar-satellite matched data sets and developed for producing large-scale and long-term rainfall estimation for climate applications. Therefore it is inevitable to produce artificial rain area with a weak rain rate as much as 1.0 ㎜/hr when this technique is applied to estimate an instantaneous rainfall. This problem is correctable by adopting a suitable cutoff rain rate value such as 1.0 ㎜/hr. Given the limitations associated with the 3-D LUT technique, however, it captured peak rainfalls and accumulative rainfall with better agreement than other techniques in both cases of heavy rain (Figure 2) and moderate rain (Figure 3). It is proved that this technique appears promising for monitoring severe weather.

6. Concluding Remarks

Using the three IR channels of the GMS-5, the feasibility of rainfall estimation was studied using collocated radar data as a ground truth. In this study, three variables of TB_{11}, TB_{11-12}, $TB_{11-6.7}$ were selected and used to compute probability of rain and mean rain rate. A new rainfall algorithm, 3-D LUT, was proposed and compared with CST and GPI for the case of severe weather of typhoon. The error and scatter of the 3-D LUT estimations were relatively large, but 3-D LUT shows better results than other techniques.

Acknowledgments

The author wishes to express his sincere appreciation to Tsuyoshi Nitta, R.F. Adler and D.W. Martin for providing helpful discussions and information on the negative $TB_{11-6.7}$.

REFERENCES

Ackerman, S.A., 1996. Global satellite observations of negative brightness temperature differences between 11 and 6.7 ㎛ (in press)

Adler, R.F. and A.J. Negri, 1988. A satellite infrared technique to estimate tropical convective and stratiform rainfall. *J. of Appl. Meteor..*, **27**, 30-51.

Arkin, P.A. and B.N. Meisner, 1987. The relationship between large-scale convective rainfall and cold cloud over the western hemisphere during 1982-1984. *Mon. Wea. Rev.*, **115**, 51-74

Griffith, C.G., W.L. Woodley, P.G. Grube, D.W. Martin, J. Stout and D.N. Sikdar, 1978. Rain Estimation from geosynchronous satellite imagery-visible and infrared studies, *Mon. Wea. Rev.*, **112**, 56-75

Inoue, T, 1987a. A cloud type classification with NOAA 7 split-window measurements. *J. Geophys. Res.*, **92**, 3991-4000

Inoue, T, 1987b. An instantaneous delineation of convective rainfall area using split window data of NOAA-7 AVHRR. *J. Meteor. Soc. Japan*, **65**, 469-481

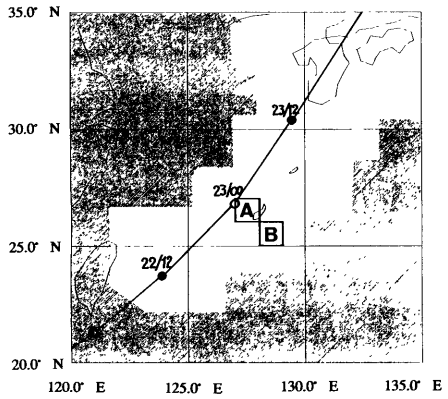

Fig. 1. A region of data sets for geographically matched GMS-5 IR data and a composite digital radar data.
A white area is a coverage of radar observation for effective beam hight of 4,000m.
A solid line shows a route of typhoon "RYAN(T9514)".
Bold number refer to the position at the date and time (22/12 is at 12 UTC on 22 September 1995).
Two 1°×1° squares, centered at A (26.5° N, 127.5° E) and B(25.5° N, 128.5° E) respectively, are selected for the validation of rainfall estimation techniques.

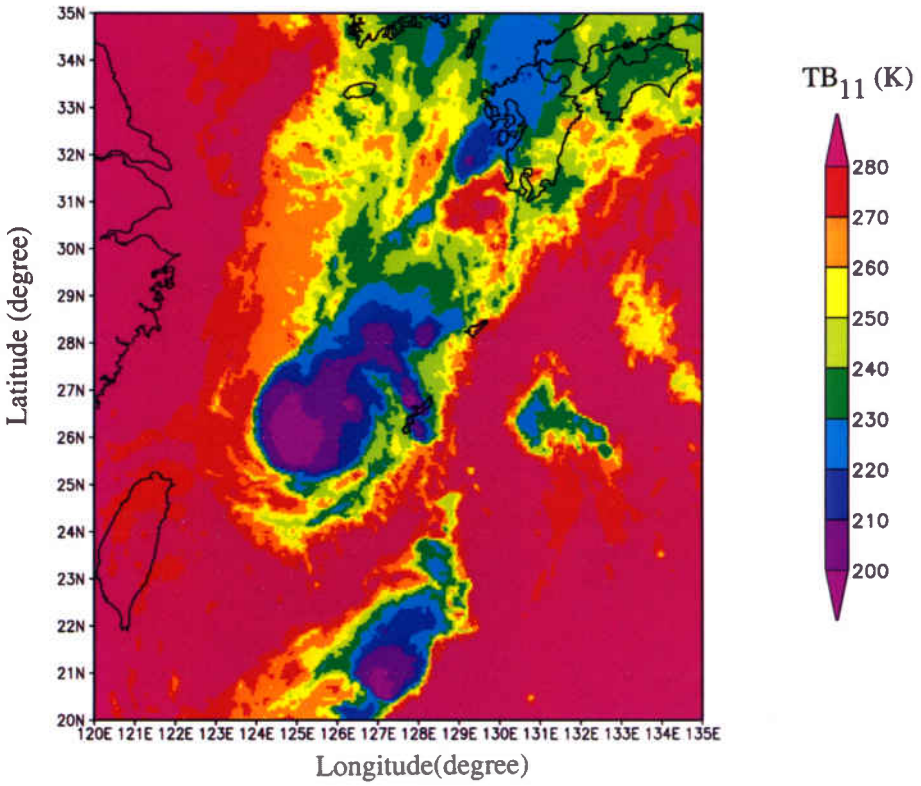

Fig. 2.1. The GMS-5 "false-color" image of infrared (IR) 11 ㎛ brightness temperature (TB_{11}) at 00 UTC on 23 September 1995 in the case of typhoon "RYAN (T9514)".

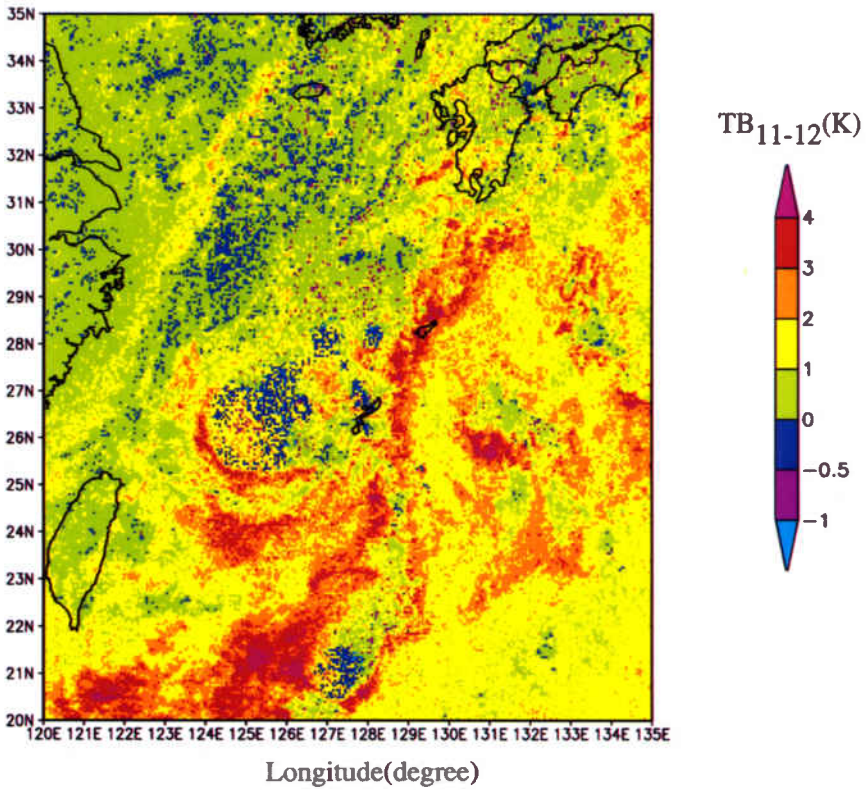

Fig. 2.2. The GMS-5 "false-color" image of IR TB difference between 11 ㎛ and 12 ㎛ (TB_{11-12}) at 00 UTC on 23 September 1995 in the case of typhoon "RYAN (T95114)".

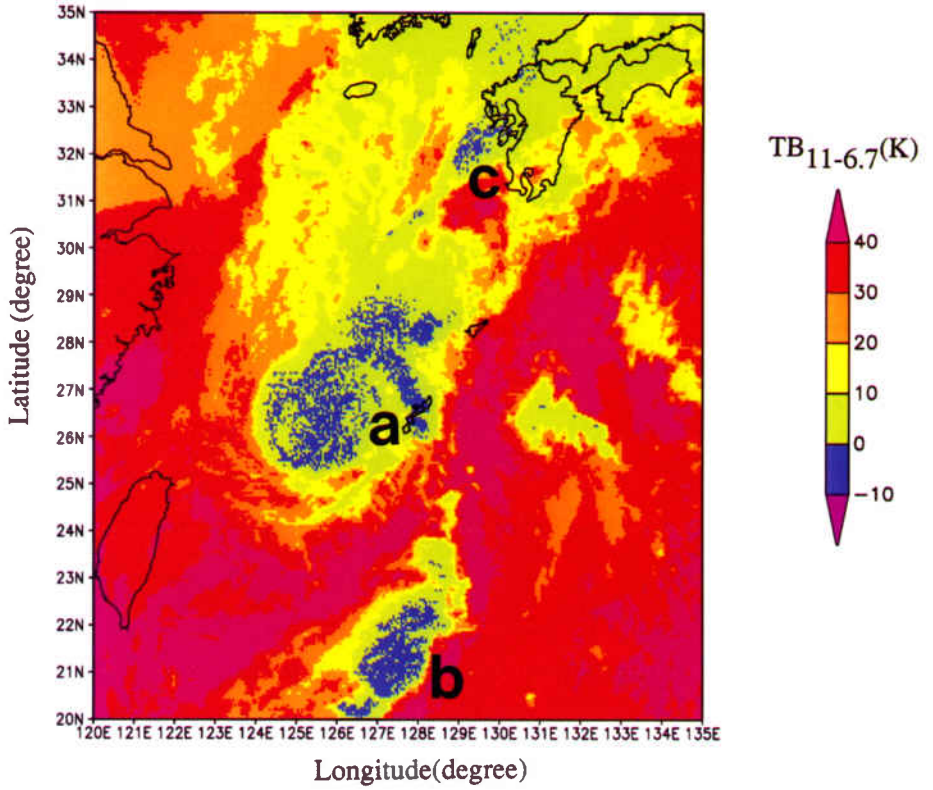

Fig. 2.3. The GMS-5 "false-color" image of IR TB difference between 11 μm and 6.7 μm ($TB_{11-6.7}$) at 00 UTC on 23 September 1995 in the case of typhoon "RYAN (T95114)".

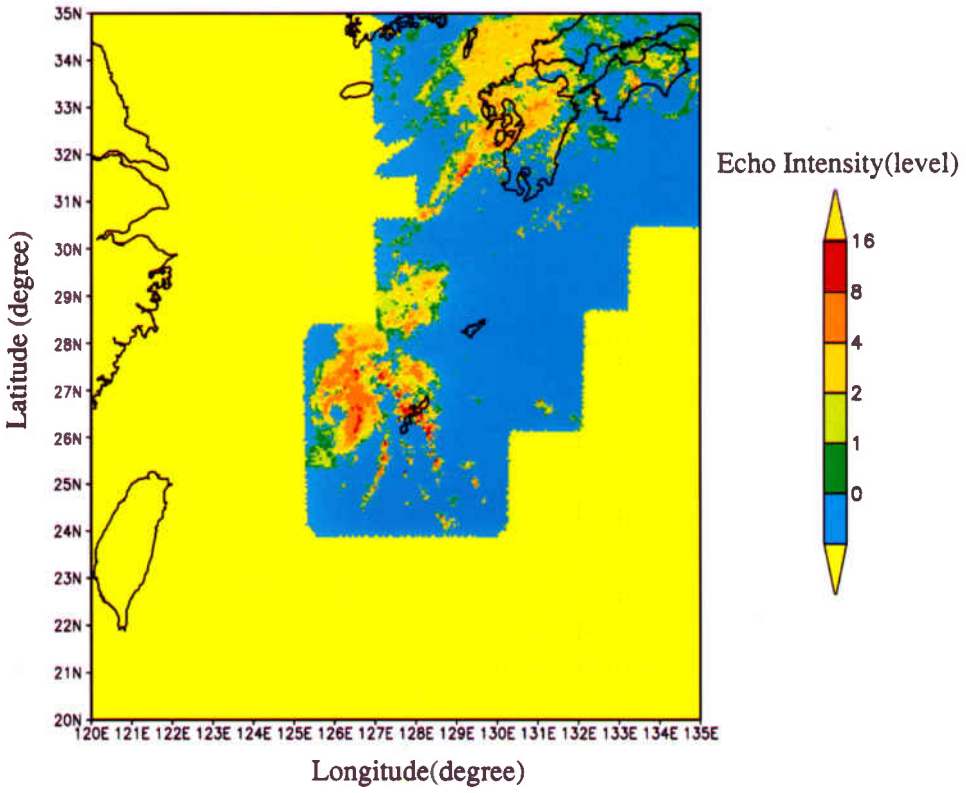

Fig. 3. The radar "false-color" image of digitized echo intensity for 16 levels obtained through Japan Meteorological Agency (JMA) weather radar network at 00 UTC on 23 September 1995 in the case of typhoon "RYAN (T9514)". where "blue" area shows "no rain" area

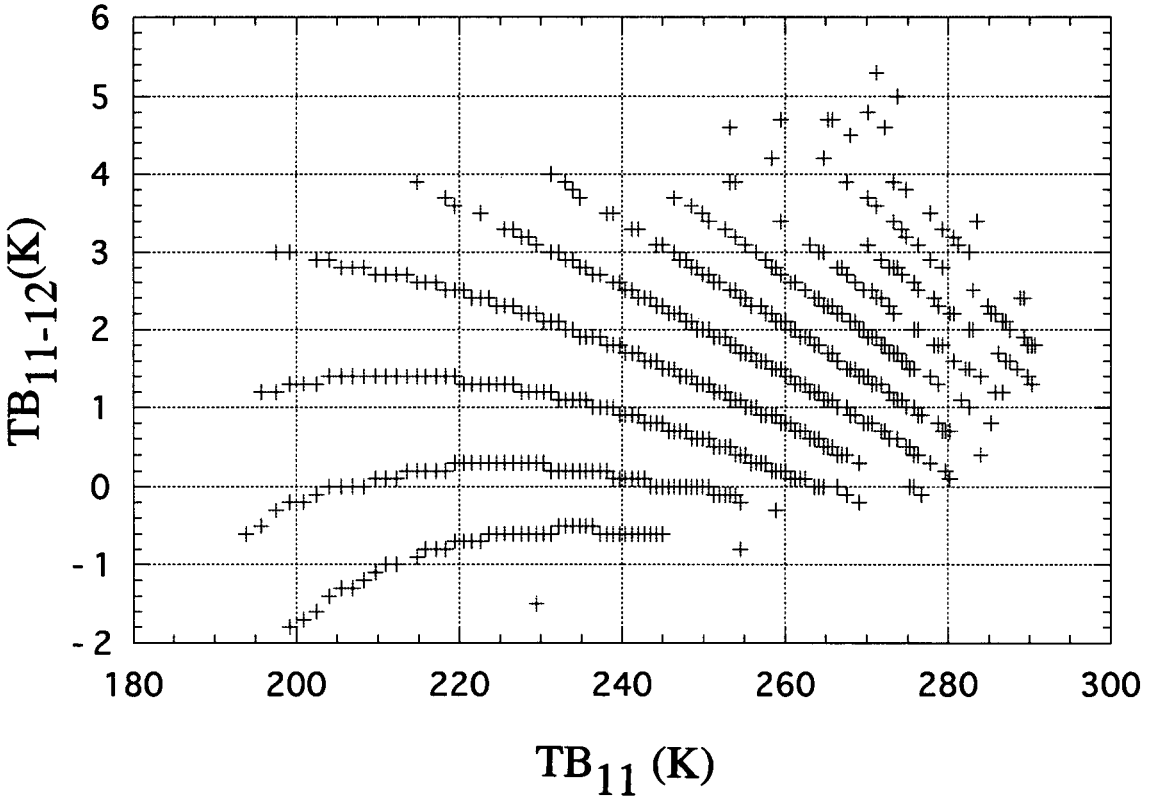

Fig. 4.1. The scatter diagram of raining pixels
at 00 UTC on 23 September 1995 in the case of typhoon "RYAN (T95114)".

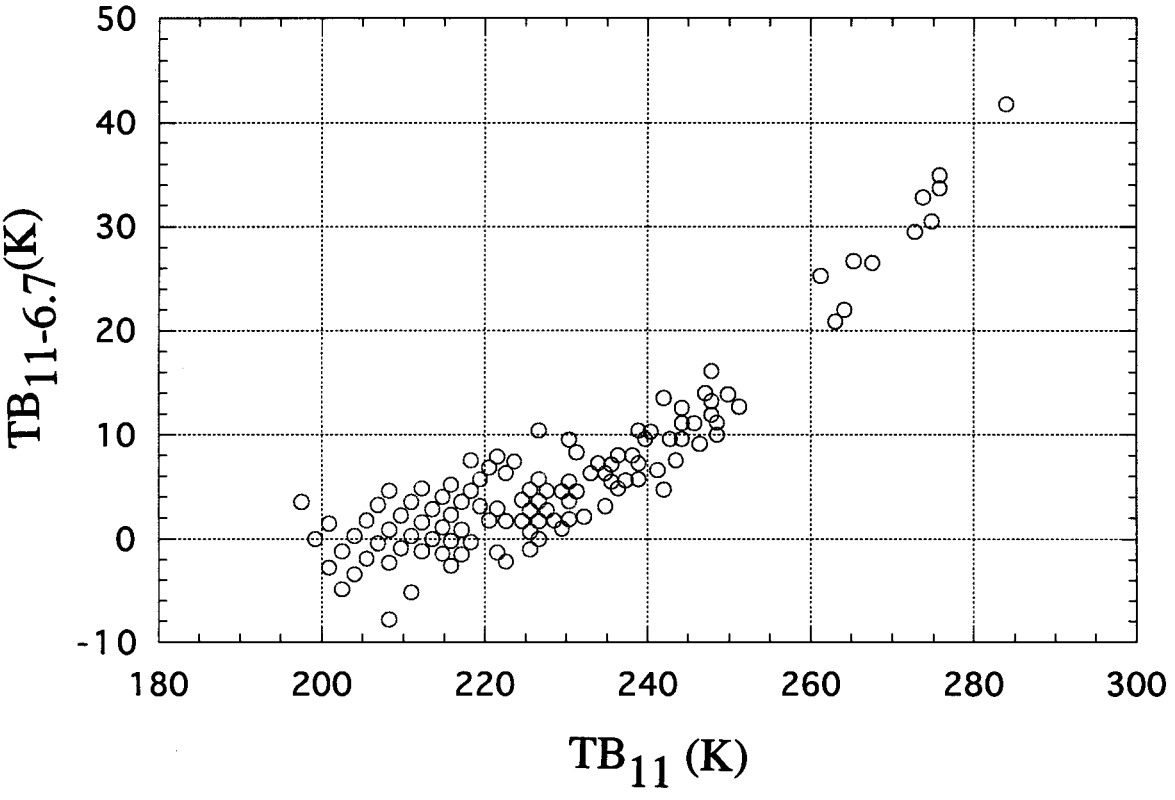

Fig. 4.2. The scatter diagram of "heavy (over 20.0 ㎜/hr)" raining pixels
at 00 UTC on 23 September 1995 in the case of typhoon "RYAN (T9514)".

```
                       TB11 (DEG. C)
         >20.0     0.0   -20.0   -40.0   -60.0   -80.0  -100.0
           +-------+-------+-------+-------+-------+-------+--

TB11 - TB12

     <-10.0    - - - - - - - - - - - - - - - - - - - - - - - - - -
-10.0< -9.0    - - - - - - - - - - - - - - - - - - - - - - - - - -
-9.0 < -8.0    - - - - - - - - - - - - - - - - - - - - - - - - - -
-8.0 < -7.0    - - - - - - - - - - - - - - - - - - - - - - - - - -
-7.0 < -6.0    - - - - - - - - - - - - - - - - - - - - - - - - - -
-6.0 < -5.0    - - - - - - - - - - - - - - - - - - - - - - - - - -
-5.0 < -4.0    - - - - - - - - - - - - - - - - - - - - - - - - - -
-4.0 < -3.0    - - - - - - - - - - - - - - - - - - - - - - - - - -
-3.0 < -2.0    - - - - - - - 7 9 6 9 7 8 - - - - - - - - - - - - -
-2.0 < -1.0    - - - 6 6 6 6 6 6 6 6 7 7 7 8 7 8 8 9 9 - - - - - -
-1.0 <  0.0    0 0 1 2 3 3 3 4 4 5 4 5 6 6 6 6 7 8 8 9 9 A - - - -
 0.0 <  1.0    0 0 1 2 2 2 3 3 4 4 4 5 5 5 6 6 7 8 8 8 9 - - - - 2
 1.0 <  2.0    0 1 1 1 1 1 2 2 2 3 3 4 4 4 5 6 6 8 8 9 9 A - - - -
 2.0 <  3.0    0 1 1 1 1 1 1 1 1 2 2 2 3 3 4 4 5 7 8 7 - - - - - -
 3.0 <  4.0    0 0 1 1 1 1 1 1 1 1 2 2 2 2 2 3 5 7 8 9 9 - - - - -
 4.0 <  5.0    - 0 0 1 1 1 1 1 1 1 1 1 2 2 2 2 4 4 - - - - - - - -
 5.0 <  6.0    - - 1 0 0 1 1 1 1 2 2 2 2 1 1 2 3 - - - - - - - - -
 6.0 <  7.0    - - - 1 0 0 1 1 1 2 3 2 1 2 0 0 - - - - - - - - - -
 7.0 <  8.0    - - - - 0 0 1 3 1 0 2 2 1 0 - - - - - - - - - - - -
 8.0 <  9.0    - - - - - 0 1 - - - - - - - - - - - - - - - - - - -
 9.0 <         - - - - - - - - - - - - - - - - - - - - - - - - - -
```

Table 1 a.

2-D matrix of probability of rain (PoR) whose axes of TB_{11} and TB_{11-12} ($\times 10\%$). "1" means 10% and "A" means 100%

```
                       TB11 (DEG. C)
         >20.0     0.0   -20.0   -40.0   -60.0   -80.0  -100.0
           +-------+-------+-------+-------+-------+-------+--

TB11 - TB12

     <-10.0    - - - - - - - - - - - - - - - - - - - - - - - - - -
-10.0< -9.0    - - - - - - - - - - - - - - - - - - - - - - - - - -
-9.0 < -8.0    - - - - - - - - - - - - - - - - - - - - - - - - - -
-8.0 < -7.0    - - - - - - - - - - - - - - - - - - - - - - - - - -
-7.0 < -6.0    - - - - - - - - - - - - - - - - - - - - - - - - - -
-6.0 < -5.0    - - - - - - - - - - - - - - - - - - - - - - - - - -
-5.0 < -4.0    - - - - - - - - - - - - - - - - - - - - - - - - - -
-4.0 < -3.0    - - - - - - - - - - - - - - - - - - - - - - - - - -
-3.0 < -2.0    - - - - - - - G B I A F D - - - - - - - - - - - - -
-2.0 < -1.0    - - - E A D D F E D F E D C F C 9 B D F - - - - - -
-1.0 <  0.0    - 3 5 8 7 9 7 7 7 6 6 6 7 7 8 9 9 B A D 8 8 - - - -
 0.0 <  1.0    3 4 7 7 7 7 6 5 5 5 5 5 5 6 7 7 9 B D E L - - - - 6
 1.0 <  2.0    3 5 7 8 9 8 7 6 6 6 6 6 6 6 7 8 9 B C C 8 7 - - - -
 2.0 <  3.0    3 6 6 7 7 7 7 8 8 7 7 7 7 8 8 9 B D D F - - - - - -
 3.0 <  4.0    1 5 5 6 6 7 7 7 8 7 8 8 8 9 A B 9 I E 9 8 - - - - -
 4.0 <  5.0    - - 5 6 6 7 7 6 8 8 8 8 8 A 8 6 5 6 - - - - - - - -
 5.0 <  6.0    - - - 5 7 8 6 9 8 7 9 8 9 8 9 C 2 - - - - - - - - -
 6.0 <  7.0    - - - - 1 2 6 8 9 9 C C H R - - - - - - - - - - - -
 7.0 <  8.0    - - - - - - 2 6 - - H 3 - - - - - - - - - - - - - -
 8.0 <  9.0    - - - - - - - - - - - - - - - - - - - - - - - - - -
 9.0 <         - - - - - - - - - - - - - - - - - - - - - - - - - -
```

Table 1 b.

2-D matrix of mean rain rate (mRR) whose axes of TB_{11} and TB_{11-12} (mm/hr). "1" means 1.0 mm/hr, "A" means 10.0 mm/hr, "B" means 11.0 mm/hr, and so on.

```
                       TB11 (DEG. C)
         >20.0     0.0   -20.0   -40.0   -60.0   -80.0  -100.0
           +-------+-------+-------+-------+-------+-------+--

TB11 - TB6.7

     <-10.0    - - - - - - - - - - - - - - - - 5 - - - - - - - - 5
-10.0< -8.0    - - - - - - - - - - - - - - 6 7 7 8 - - - - - - - -
-8.0 < -6.0    - - - - - - - - - - - - - - 5 6 6 7 7 7 - - - - - -
-6.0 < -4.0    - - - - - - - - - - - - 6 6 6 6 6 7 7 8 8 - - - - -
-4.0 < -2.0    - - - - - - - - - - - 6 6 6 6 6 6 7 7 8 8 9 - - - -
-2.0 <  0.0    - - - - - - - - - - - 6 5 6 6 6 6 7 8 8 8 9 - - - -
 0.0 <  2.0    - - - - - - - - - - 6 6 5 6 6 6 6 7 8 8 8 - - - - 6
 2.0 <  4.0    - - - - - - - - - 6 5 6 6 6 6 6 6 7 7 8 8 9 - - - -
 4.0 <  6.0    - - - - - - - - - 6 5 6 6 6 5 5 6 7 8 8 9 9 - - - -
 6.0 <  8.0    - - - - - - - - 5 5 5 6 5 5 5 5 6 7 8 8 9 - - - - -
 8.0 < 10.0    - - - - - 2 - 4 5 5 6 5 4 4 5 5 7 7 - - - - - - - -
10.0 < 12.0    - - - - 2 - 4 5 5 5 5 4 4 4 5 6 7 - - - - - - - - -
12.0 < 14.0    - - - - 2 2 5 5 5 5 5 4 4 4 5 6 - - - - - - - - - -
14.0 < 16.0    - - - 1 2 3 4 4 5 5 4 4 4 4 5 - - - - - - - - - - -
16.0 < 18.0    - - - 1 2 4 4 4 5 4 3 4 4 5 5 - - - - - - - - - - -
18.0 < 20.0    - - 1 2 2 4 4 4 4 3 3 4 4 4 - - - - - - - - - - - -
20.0 < 22.0    - - 1 2 4 4 4 4 3 3 3 4 5 - - - - - - - - - - - - -
22.0 < 24.0    - - 2 3 4 3 3 3 3 3 4 4 4 - - - - - - - - - - - - -
24.0 < 26.0    - 3 2 3 4 3 3 3 3 3 4 5 - - - - - - - - - - - - - -
26.0 < 28.0    6 3 2 3 3 3 3 3 3 3 4 4 - - - - - - - - - - - - - -
28.0 <         2 2 2 3 3 3 3 3 3 4 6 - - - - - - - - - - - - - - -
```

Table 2 a.

2-D matrix of probability of rain (PoR) whose axes of TB_{11} and $TB_{11-6.7}$ ($\times 10\%$). "1" means 10% and "A" means 100%

```
                       TB11 (DEG. C)
         >20.0     0.0   -20.0   -40.0   -60.0   -80.0  -100.0
           +-------+-------+-------+-------+-------+-------+--

TB11 - TB6.7

     <-10.0    - - - - - - - - - - - - - - - - E - - - - - - - - 6
-10.0< -8.0    - - - - - - - - - - - - - - P W O K - - - - - - - -
-8.0 < -6.0    - - - - - - - - - - - - - - C E K H I Q - - - - - -
-6.0 < -4.0    - - - - - - - - - - - - F J C C C E K I K - - - - -
-4.0 < -2.0    - - - - - - - - - - - J M G D B B B E E D 8 - - - -
-2.0 <  0.0    - - - - - - - - - - - I B B A 9 9 A C D C 7 - - - -
 0.0 <  2.0    - - - - - - - - - - G C A 7 7 7 8 A C B 7 - - - - 6
 2.0 <  4.0    - - - - - - - - - E E 9 6 5 6 7 9 B D C 7 8 - - - -
 4.0 <  6.0    - - - - - - - - - C B 6 5 5 7 9 C F E 7 9 9 - - - -
 6.0 <  8.0    - - - - - - - - 8 A 7 5 5 7 9 D F N M 5 8 - - - - -
 8.0 < 10.0    - - - - - 1 - 3 A 7 5 5 7 9 D G R O - - - - - - - -
10.0 < 12.0    - - - - 1 - 4 6 7 5 5 6 9 C F J O - - - - - - - - -
12.0 < 14.0    - - - - 1 2 A 5 6 5 6 7 9 D F Q - - - - - - - - - -
14.0 < 16.0    - - - 2 3 8 6 5 5 5 7 9 B F H - - - - - - - - - - -
16.0 < 18.0    - - - 1 2 7 7 5 5 6 7 9 B H / - - - - - - - - - - -
18.0 < 20.0    - - 1 1 3 8 6 5 6 7 8 C H D - - - - - - - - - - - -
20.0 < 22.0    - - 1 2 7 8 6 6 7 7 A C I - - - - - - - - - - - - -
22.0 < 24.0    - - 1 4 9 8 6 7 7 8 C D 7 - - - - - - - - - - - - -
24.0 < 26.0    - 2 1 5 8 7 7 8 7 A D G - - - - - - - - - - - - - -
26.0 < 28.0    1 1 4 7 9 7 7 7 9 A J 5 - - - - - - - - - - - - - -
28.0 <         3 5 7 8 7 7 7 8 C F Z - - - - - - - - - - - - - - -
```

Table 2 b.

2-D matrix of mean rain rate (mRR) whose axes of TB_{11} and $TB_{11-6.7}$ (mm/hr). "1" means 1.0 mm/hr, "A" means 10.0 mm/hr, "B" means 11.0 mm/hr, and so on.

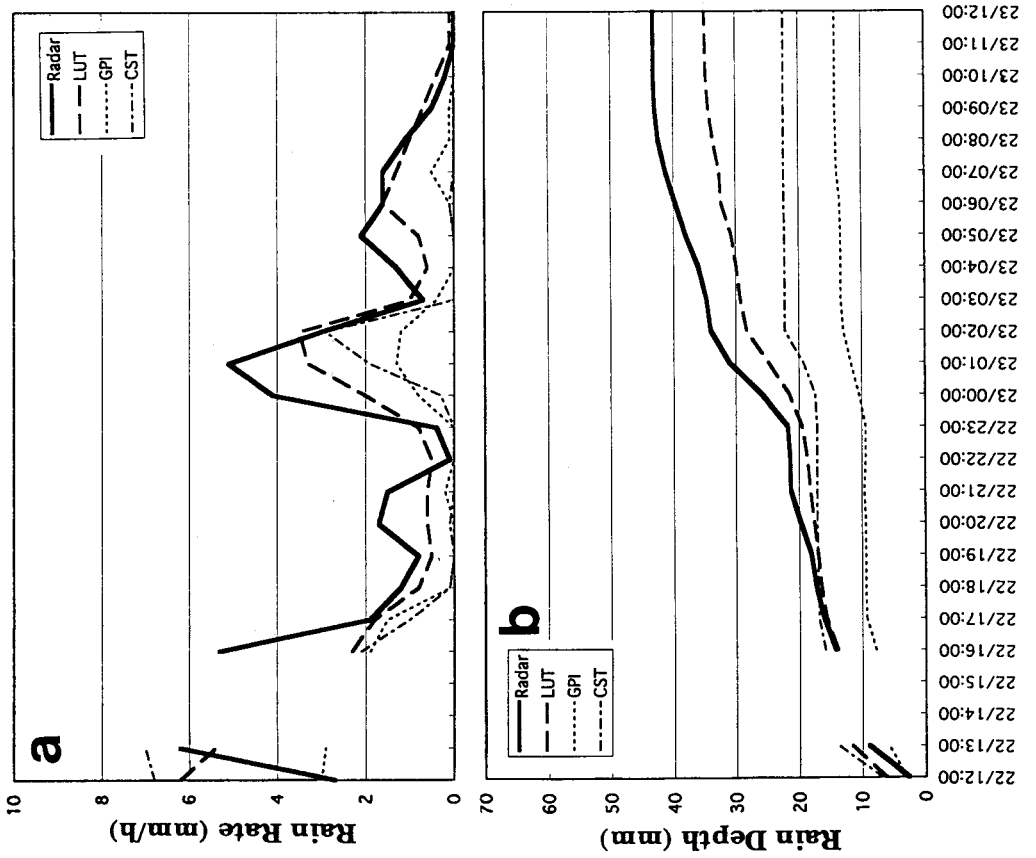

Fig. 5. A representative comparison of rain estimation and radar ground truth for 1°×1° squares centered at (26.5°N, 127.5°E), described as "A" in Figure 1, from 12 UTC, 22 September through 12 UTC, 23 September 1995. Hourly (a) and accumulative (b) rainfalls are shown.

Fig. 6. As in Fig. 2 except box "B", (25.5°N, 128.5°E).

where

Radar : radar ground truth

LUT : 3-D LUT technique estimation

CST : CST technique estimation (Adler, 1988)

GPI : GPI technique estimation (Arkin, 1987)

GMS-5の赤外スプリット及び水蒸気チャンネル観測データを用いた降雨推定

操野　年之

GMS-5の赤外チャンネル観測データを用いた降雨推定の統計的な特性について、約2カ月分のGMS-5の赤外データと気象レーダーデータを重ね合わせたデータセットにもとづき調査した。このデータセットを用いて、「降雨確率」及び「平均降雨強度」と赤外3チャンネルのデータ（11μmチャンネルの輝度温度(TB_{11})、11μmと12μmチャンネルの輝度温度の差分（TB_{11-12}）及び11μmと6.7μmチャンネルの輝度温度の差分（$TB_{11-6.7}$))との関係について調査したところ、以下のことが解った。

(1) GMS-5のTB_{11-12}は降雨を伴わない薄い巻雲の除去に有効である。

(2) GMS-5の$TB_{11-6.7}$は強い降雨を伴う発達した積乱雲の抽出に有効である。

今回の調査で作成した「降雨確率」及び「平均降雨強度」と赤外データとの関係を用いて経験的な降雨推定手法（3-DLUT）を開発した。既存の赤外チャンネルを用いた降雨推定手法と比較したところ、3-DLUTの推定誤差及び分散は、他の推定手法と同様に比較的大きいが、時系列で比較すると、降雨のピーク及び積算降雨量については最も良い精度で推定していることが解った。